ACS APPLIED MATERIALS & INTERFACES

Research Article

www.acsami.org

# Needle-like $Co_3O_4$ Anchored on the Graphene with Enhanced Electrochemical Performance for Aqueous Supercapacitors

Qun Guan,[†,‡,§] Jianli Cheng,[‡,§] Bin Wang,[*,‡,§] Wei Ni,[‡,§] Guifang Gu,[‡,§] Xiaodong Li,[‡,§] Ling Huang,[‡,§] Guangcheng Yang,[‡,§] and Fude Nie[*,‡,§]

[†]Southwest University of Science and Technology, 643000 Mianyang, PR China

[‡]Institute of Chemical Materials, China Academy of Engineering Physics, Mianyang 621900, China

[§]New Material Center of Sichuan Province, Mianyang 621900, China

Supporting Information

**ABSTRACT:** We synthesized the needle-like cobalt oxide/graphene composites with different mass ratios, which are composed of cobalt oxide ($Co_3O_4$ or CoO) needle homogeneously anchored on graphene nanosheets as the template, by a facile hydrothermal method. Without the graphene as the template, the cobalt precursor tends to group into urchin-like spheres formed by many fine needles. When used as electrode materials of aqueous supercapacitor, the composites of the needle-like $Co_3O_4$/graphene (the mass ratio of graphene oxide(GO) and $Co(NO_3)_2{\cdot}6H_2O$ is 1:5) exhibit a high specific capacitance of 157.7 F $g^{-1}$ at a current density of 0.1 A $g^{-1}$ in 2 mol $L^{-1}$ KOH aqueous solution as well as good rate capability. Meanwhile, the capacitance retention keeps about 70% of the initial value after 4000 cycles at a current density of 0.2 A $g^{-1}$. The enhancement of excellent electrochemical performances may be attributed to the synergistic effect of graphene and cobalt oxide components in the unique multiscale structure of the composites.

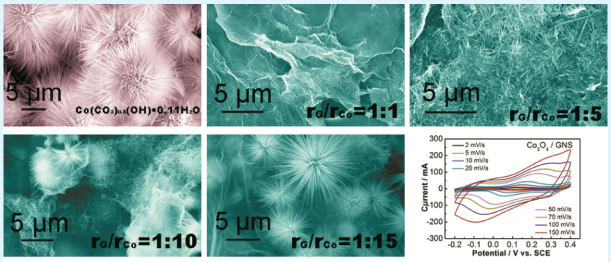


**KEYWORDS:** *needle-like $Co_3O_4$, graphene, aqueous supercapacitor, electrochemical performance, needle-like CoO, urchin-like spheres*

## 1. INTRODUCTION

Fossil fuel depletion, environmental pollution, and global warming have led to significant interest in developing green and sustainable energy storage systems.[1−3] Among various energy storage systems, supercapacitor is considered as one of the most promising candidates due to its high power density, long life cycles, and bridging the power/energy gap between traditional dielectric capacitors and batteries/fuel cells.[4]

Supercapacitor is generally classified into electrical double-layer capacitor (EDLC) and pseudocapacitor by charge−discharge mechanisms.[4,5] EDLCs usually have a high power density with low specific capacitance due to commonly using carbon materials as the electrode including active carbon[5] and carbon nanotubes.[6] Meanwhile, the pseudocapacitors based on transition metal oxides, such as $RuO_2$,[7] $Co_3O_4$,[3,8] $MnO_2$,[9] NiO,[10] and $MoO_2$,[11] have a higher energy density with poor cycling stability which can store the charge in a faradic process.[7] Among these, $Co_3O_4$ is being studied as a candidate material for pseudocapacitor electrode because it has a high theoretical specific capacitance and good electrochemical capability.[12] However, due to limited capacitance or energy density and poor cycling stability, exploring the new cobalt oxide-based composite materials for the supercapacitor has been extensively investigated in recent years.[13−15] A strategy is to grow or anchor $Co_3O_4$ onto carbon-based material to obtain the composites, which can combine the double-layer capacitance and high electrical conductivity of graphene with higher pesudocapacitance of $Co_3O_4$ to the composites at the same time.[16]

Graphene nanosheets (GNS) have emerged as a promising candidate for supercapacitor due to its extremely high specific surface area, excellent electronic conductivity, and superior intrinsic mechanical strength.[17−20] As a result, the composites of $Co_3O_4$ and graphene materials have attracted many research interests in order to get superior performance. Chen et al.[21] reported that graphene was deposited on nickel foams by an electrophoretic deposition method, which can deliver a specific capacitance of 164 F $g^{-1}$ and keep capacitance retention of 65% after 700 cycles. The multilayer graphene-based supercapacitor with a capacitance of 117 F $g^{-1}$ in aqueous $H_2SO_4$ solution has been reported.[22] The composite of reduced graphene oxide (rGO) platelets into the $Co_3O_4$ scroll has been prepared through a two-step surfactant-assisted method, showing a large specific capacitance of 163.8 F $g^{-1}$ in a 6 mol $L^{-1}$ KOH solution.[23]

Although some achievements have been made, synthesis of GNS-based materials by an environment-friendly and effective approach is still a challenge. Very recently, we synthesized

Received: February 13, 2014
Accepted: April 9, 2014
Published: April 9, 2014

   dx.doi.org/10.1021/am5009369 | ACS Appl. Mater. Interfaces 2014, 6, 7626−7632

carbon-coated $SnO_2$/GNS composites by a one pot hydrothermal approach, which can effectively prevent $SnO_2$ to be detached and exhibit better cycling performance.[24] Meanwhile, we explored a simple solvothermal method to directly self-assemble three-dimensional (3-D) $V_2O_5$ nanosheets/rGO hierarchical composites.[25]

To the best of our knowledge, the needle-like $Co_3O_4$ anchored on GNS as electrode materials of durable high-performance supercapacitors have not been reported yet. In this work, we employed a facile hydrothermal treatment of graphene oxide (GO) and cobalt nitrate hexahydrate with different mass ratios to synthesize the needle-like $Co_3O_4$ assembled on the GNS, which is composed of in situ anchoring the needle-like $Co_3O_4$ on the surface of GO nanosheets. Without the template of graphene, the cobalt oxide tends to group into urchin-like spheres formed by many fine needles. The electrochemical performance reveals that the needle-like $Co_3O_4$/GNS composites not only exhibit good pseudocapacitive behavior but also have a good cycling stability, which can keep capacitance retention of 70% after 4000 cycles.

## 2. EXPERIMENTAL SECTION

All the chemical reagents used in this study are of analytical grade and used as received without further purification. All aqueous solutions are prepared with deionized (DI) water.

**2.1. Synthesis of Graphene Oxide (GO).** In a typical synthesis, GO was prepared by a modified Hummers method.[3] First, preoxidized graphite was prepared. A total of 5 g of graphite powder was placed in a mixed solution of concentrated $H_2SO_4$ (60 mL), $K_2S_2O_8$ (5 g) and $P_2O_5$ (5 g) at 80 °C. The resultant dark blue mixture was cooled to room temperature, and then carefully washed with DI water. The preoxidized product was dried in an oven overnight at 80 °C. Then, 2.5 g of preoxidized graphite was added to cold concentrated $H_2SO_4$ in a water−ice bath. A total of 7.5 g of $KMnO_4$ was slowly added to the mixture under stirring and then diluted with 230 mL of DI water. After that, the mixture was stirred at 95 °C for 1.5 h followed by adding 30 wt % $H_2O_2$ solution and filtrated and washed by HCl three times. The GO dispersion was then subjected to dialysis to completely remove metal ions and acids.

**2.2. Synthesis of $Co_3O_4$/ Graphene.** The needle-like precursor $Co(CO_3)_{0.5}(OH)\cdot 0.11H_2O$/reduced graphene oxide (rGO) was synthesized by a simple hydrothermal method. In a typical preparation process, 0.29 g of $Co(NO_3)_2\cdot 6H_2O$, 0.12 g of $NH_4F$, and 0.30 g of urea were dissolved in 10 mL of deionized water. Then the required amount of GO dispersion (5.5 mg $mL^{-1}$) was sonicated for 30 min and dropped into the above solution. The subsequently mixed suspension was stirred for 1 h and sonicated for 5 min. The resulting solution was transferred to a Teflon lined autoclave and heated at 120 °C for 5 h. Then, the solid precipitate was obtained by centrifuge with repeated washing with DI water and ethanol, respectively. After drying at 60 °C for 12 h, the solid was heated to 300 °C at a rate of 1 °C $min^{-1}$ for 3 h under $N_2$ atmosphere. The needle-like $Co_3O_4$/GNS composites were obtained. In our experiments, the mass ratios of GO and $Co(NO_3)_2\cdot 6H_2O$ ($r_G/r_{Co}$, weight ratio) were controlled as 1:1, 1:5, 1:10, and 1:15. For the preparation, pure needle-like $Co_3O_4$ and pure GNS were also prepared by the same procedure in the absence of the GNS and $Co_3O_4$, respectively.

**2.3. Materials Characterization.** The chemical composition of the samples was determined by X-ray diffraction (XRD, PANalytical, X'Pert PRO, Cu K$\alpha$). The morphology of the synthesized products was examined using field emission scanning electron microscopy (FESEM, Carl Zeiss SMT Pte Ltd., Ultra 55), atomic force microscopy (AFM) image taking in tapping mode with the SPI 3800N from NSK and transmission electron microscopy (TEM, Carl Zeiss SMT Pte Ltd., Libra 200 FE, 200 kV). Thermogravimetric (TG) analysis was carried out on a SDT Q600 instrument to determine the weight ratio of GNS to $Co_3O_4$ in a temperature range of 30−800 °C. Raman spectroscopy was recorded from 400 to 3600 $cm^{-1}$ on a Renishaw Invia Raman microscope excited by an argon ion laser beam (514.5 nm, 20 mW). Fourier-transform infrared (FT-IR) spectra of KBr powder pressed pellets was recorded on a Spectrum One FTIR (PerkinElmer Instrument Co.) in the range of 4000−500 $cm^{-1}$. X-ray photoelectron (XPS) spectra were acquired with an Axis Ultra DLD (Shimadzu-Kratos Co.).

**2.4. Electrochemical Measurements.** The electrochemical behavior of the samples was tested by a three-electrode cell in aqueous 2 mol $L^{-1}$ KOH electrolyte solution at room temperature. The working electrode was prepared by mixing 75 wt % of the needle-like $Co_3O_4$/GNS composites, 15 wt % of the carbon black, and 10 wt % of the binder (polytetrafluoroethylene, PTFE, Aldrich). This mixture was then pressed onto the nickel foam at a pressure of 10 MPa and dried at 100 °C under vacuum. As the counterpart, pure needle-like $Co_3O_4$ was prepared by the same method as describe above. Pt foil and standard calomel electrode (SCE) are used as the counter electrode and the reference electrode, respectively. The cyclic voltammogram (CV) and electrochemical impedance spectroscopy (EIS) tests were carried out using a VSP (Bio-Logic SAS) electrochemical workstation. Galvanostatic charge/discharge cycling measurements were taken by the CT2001A battery program controlling test system (China-Land Co., Ltd.). According to galvanostatic charge/discharge cycling measurements, specific capacitance (Cs) can be calculated by the following equation, $Cs = I\Delta t/\Delta U$ (eq 1), where $I$ is current density (A $g^{-1}$), $\Delta t$ (s) is the discharge time, and $\Delta U$ is the voltage difference (V) from the end of charge drop to the end of the discharge process.

## 3. RESULTS AND DISCUSSION

The fabrication processes are illustrated in Figure 1. First, GO was ultrasonically dispersed in DI water. The graphite oxide was

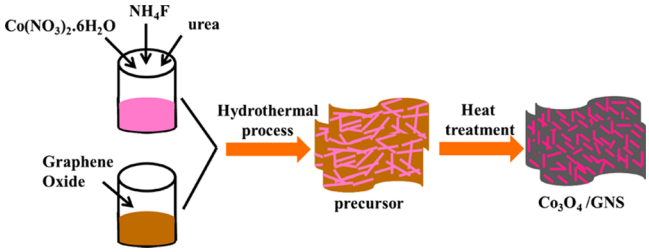


**Figure 1.** Schematic illustration of the preparation processes of the needle-like $Co_3O_4$/GNS composite.

exfoliated to GO layers. Meanwhile, cobalt nitrate hexahydrate was dissolved with the mixture solution of ammonium fluoride and urea and then mixed with the GO solution in the PTFE autoclave. Second, in the hydrothermal process, $Co^{2+}$ intercalated into the GO nanosheets to further integrate with carboxyl and phenolic hydroxyl groups that exist on the GO sheets.[26] At the initial stages, GO nanosheets decorated with many fine nanoparticles were formed and acted as nucleation sites for further particle growth.[27,28] Then, these particles spontaneously aggregated into needle on the surface of GO nanosheets. After annealing, the precursor of $Co(CO_3)_{0.5}(OH)\cdot 0.11H_2O$/rGO composites turns to $Co_3O_4$/GNS composites.

The morphology and microstructure of pure needle-like $Co(CO_3)_{0.5}(OH)\cdot 0.11H_2O$ and needle-like $Co(CO_3)_{0.5}(OH)\cdot 0.11H_2O$/rGO composites with different mass ratios were characterized by the AFM and FESEM, as shown in Figure 2. It can be seen from the AFM in Figure 2a that the edges of the GO nanosheet with a plane dimensions of about 1−8 $\mu$m were wrinkled. The GO sheet has a lateral thickness of 1.3−1.8 nm which corresponds to multilayered GO. Seen from the SEM


dx.doi.org/10.1021/am5009369 | ACS Appl. Mater. Interfaces 2014, 6, 7626−7632

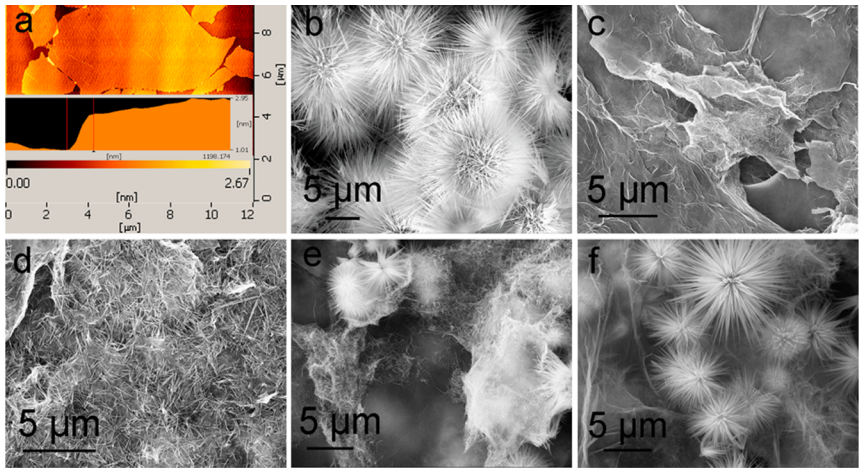


**Figure 2.** AFM image of GO (a) and pure needle-like $Co(CO_3)_{0.5}(OH)\cdot 0.11H_2O$. (b) SEM images of the needle-like $Co(CO_3)_{0.5}(OH)\cdot 0.11H_2O$/reduced GO composites (c–f) and the mass ratio of GO:$Co(NO_3)_2\cdot 6H_2O$ is (c) 1:1, (d) 1:5, (e) 1:10, (f) 1:15.

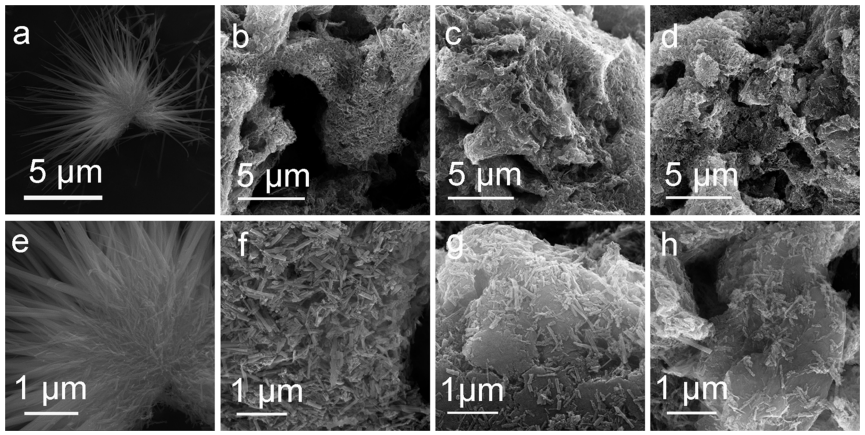


**Figure 3.** SEM images of pure $Co(CO_3)_{0.5}(OH)\cdot 0.11H_2O$ annealing at 300 °C in $N_2$ (a and e) and $Co(CO_3)_{0.5}(OH)\cdot 0.11H_2O$/rGO (GO:$Co(NO_3)_2\cdot 6H_2O$ = 1:5) annealing at 300 °C (b and f), 400 °C (c and g), 500 °C (d and h) in $N_2$.

images as shown in Figure 2b, pure $Co(CO_3)_{0.5}(OH)\cdot 0.11H_2O$ forms some uniform hierarchical urchin-like aggregate with diameters of 5–10 $\mu$m which consists of many fine needles. After being incorporated with $Co(CO_3)_{0.5}(OH)\cdot 0.11H_2O$, each $Co(CO_3)_{0.5}(OH)\cdot 0.11H_2O$/rGO composite displays an interesting and distinctive morphology. In the composite with a mass ratio of 1:1 ($r_G/r_{Co}$), a relatively less needle-like structure anchored by particles on rGO nanosheets is clearly revealed (Figure 2c). When the $r_G/r_{Co}$ is 1:5, the composites show a very uniform hierarchical needle-like $Co(CO_3)_{0.5}(OH)\cdot 0.11H_2O$ anchored on rGO nanosheets, and the sizes of needle-like $Co(CO_3)_{0.5}(OH)\cdot 0.11H_2O$ become shorter (Figure 2d). However, when the $r_G/r_{Co}$ increases to 1:10, the composites show a mixture of long needles and urchin-like spheres formed by further aggregates of the needles due to high concentration of cobalt in the solution (Figure 2e). It demonstrates that, with high concentration of cobalt salt, the cobalt precursor on the graphene tends to group into urchin-like spheres formed by many fine needles, which is well consistent with the formed precursor without the use of graphene. Obviously, the factors of self-nucleation and the assembly on the graphene competitively affected the cobalt behavior in the solution, leading to different morphologies formed on the graphene. As the mass ratio reaches 1:15, more urchin-like spheres are observed (Figure 2f). For comparison, we choose the sample obtained with $r_G/r_{Co}$ of 1:5 as the electrode material.

Subsequent thermal treatment of the needle-like $Co(CO_3)_{0.5}(OH)\cdot 0.11H_2O$/rGO with $r_G/r_{Co}$ of 1:5 in $N_2$ at different temperatures led to the formation of cobalt oxide/GNS composites. To explore the influence of heat treatment temperature on the morphology of the composites, the SEM images of the sample obtained at different temperatures are shown in Figure 3. When the precursors were annealed at 300 °C, the urchin-like structure of the $Co(CO_3)_{0.5}(OH)\cdot 0.11H_2O$ precursor is still well maintained with a shorter needle. In contrast, the composites of Co-precursor/GO were annealed at 300 °C, the urchin-like structure of the precursors disappeared, and the composite demonstrated a uniform hierarchical structure of many fine needles anchored on rGO nanosheets due to the template effect of the graphene. However, heat treatment of 400 °C makes the partial needle structure damage and break down to form small nanoparticles. This might be attributed to the process where a small part of cobalt oxide decomposed to produce $O_2$ and change to CoO, which can be seen from the XRD test. As the temperature rose to 500 °C, the needles anchored on rGO nanosheets obviously reduced.

The crystal structure of GNS, pure $Co_3O_4$, and the composites obtained before and after annealing at different temperatures (300, 400, and 500 °C) was analyzed by XRD. As


dx.doi.org/10.1021/am5009369 | ACS Appl. Mater. Interfaces 2014, 6, 7626–7632

shown in Figure 4, a small diffraction peak appears at around 11° and a broad peak locates at between 24 and 27°, which can

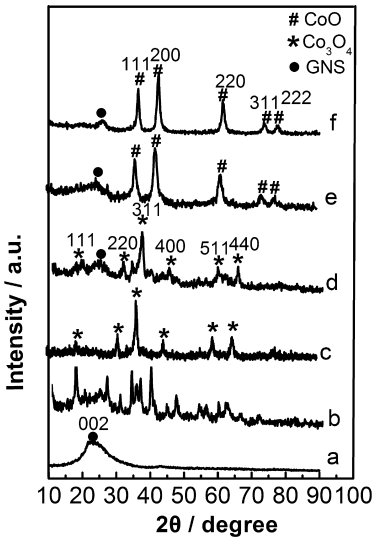


**Figure 4.** Typical XRD patterns of GNS (a), $Co(CO_3)_{0.5}(OH)\cdot 0.11H_2O$/rGO composites (b), pure $Co_3O_4$ (c), and the composites sample obtained after annealing at 300 °C (d), 400 °C (e), and 500 °C(f).

be indexed to the (001) peak of disorderedly stacked GO and the (002) peak of GNS,[29,30] respectively. For the XRD of GNS (Figure 4a), the small peak at approximately 11° disappears and a broad peak appears at approximately 22.6°, confirming the conversion of GO to GNS.[29] Most of the diffraction peaks of the composites before annealing in Figure 4b can be attributed to orthorhombic $Co(CO_3)_{0.5}(OH)\cdot 0.11H_2O$ (JCPDS card No. 48-0083). For the XRD patterns of $Co_3O_4$ (Figure 4c), the diffraction peaks can be assigned to the crystal planes of (111), (220), (311), (400), (511), and (440), respectively, which also can be observed in $Co_3O_4$/ GNS composites (Figure 4d). It is well indexed to the face-centered cubic structured $Co_3O_4$ (JCPDS card No. 42-1467, *Fd*3*m*). Besides, the diffraction peak of $Co_3O_4$/GNS composites at 24.1° can be attributed to the (002) plane of graphene.[29] The (002) peak is weaker than that of GNS, implying less restacking and agglomeration of GNS in the composites.[30] In comparison, Figure 4e,f show diffraction peaks located at 36.5°, 42.4°, 61.5°, 73.7°, and 77.5°, respectively, which can be assigned to the crystal planes of (111), (200), (220), (311), and (222) of cubic structured CoO (JCPDS card No. 43-1004, *Fm*3*m*), respectively. It confirms that the $Co_3O_4$ in the composites would turn to CoO when annealed at above 400 °C. The specific surface area of the composites was also characterized by BET measurement. As shown in Supporting Information Figure S1, the specific surface area of the needle-like $Co_3O_4$/GNS was 120.6 $m^2\ g^{-1}$, higher than those of CoO/GNS composites obtained after annealing at 400 °C (110.1 $m^2\ g^{-1}$) and CoO/GNS composites obtained after annealing at 500 °C (104.9 $m^2\ g^{-1}$). High specific surface area may help to increase contact area at the electrode and electrolyte interface, provide more surface reaction sites, and quicken diffusion kinetics, which would benefit the electrochemical performance.

To determine the carbon content of the needle-like $Co_3O_4$/GNS composites ($r_G/r_{Co}$ = 1:5), TG-DSC curves are shown in Figure 5. The TG curve exhibits a typical weight loss between

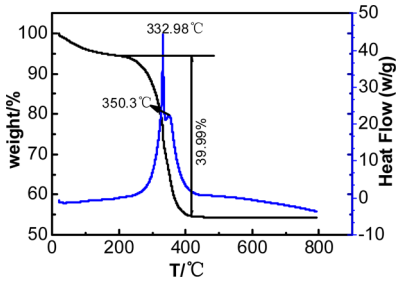


**Figure 5.** TG-DSC curves of the needle-like $Co_3O_4$/GNS composites in air.

approximately 200 and 330 °C. The abrupt weight loss between approximately 200 and 330 °C can be assigned to the decomposition reaction of labile oxygen-containing functional groups on the surface of GNS.[31] The weight loss between 330 and 440 °C can be attributed to the oxidation of the carbon skeleton.[32] Correspondingly, the DSC curve shows a strong exothermal peak centered at approximately 333 °C and a much stronger exothermal peak centered at 350.3 °C. The amount of GNS in the needle-like $Co_3O_4$/GNS composites is about 40 wt %.

To better know the structural information on needle-like $Co_3O_4$ on GNS, TEM and an elemental mapping test were carried out as shown in Figure 6. As seen from TEM image

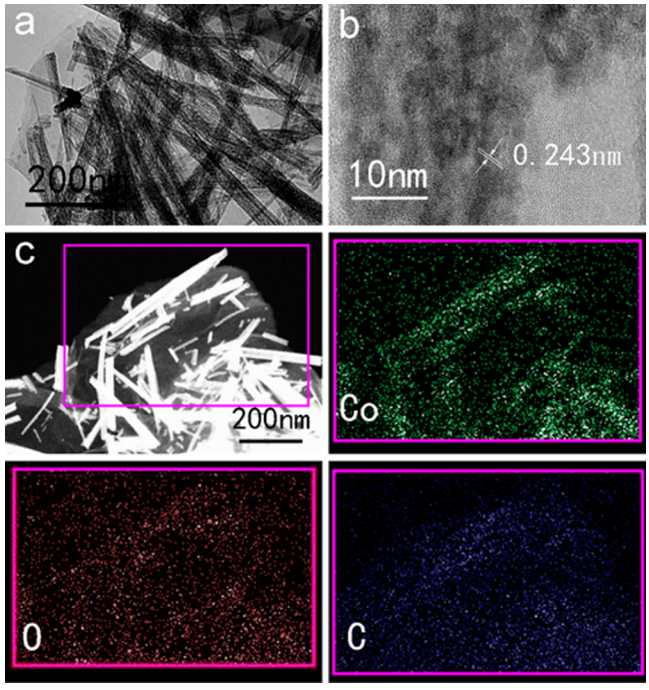


**Figure 6.** (a) TEM image of the needle-like $Co_3O_4$/GNS composites. (b) HRTEM image of the needle-like $Co_3O_4$/GNS composites. (c) HADDF STEM image and elemental mapping images of cobalt, oxygen, and carbon.

(Figure 6a), needle-like $Co_3O_4$ is well incorporated within GNS. The HRTEM image in Figure 6b clearly indicates that each building block of needle-like $Co_3O_4$ on GNS is composed of many interconnected $Co_3O_4$ nanocrystals with the sizes of 10−50 nm.[33] The interplanar distances of lattice fringes are about 0.243 nm. The presence of $Co_3O_4$ is further confirmed by elemental mappings of the composites, as shown in the


dx.doi.org/10.1021/am5009369 | ACS Appl. Mater. Interfaces 2014, 6, 7626−7632

mapping images of HADDF STEM in Figure 6c. It can be seen that the cobalt, oxygen, and carbon elements are distributed uniformly in the needle-like $Co_3O_4$/GNS composites.

The GNS from reduction of GO was also confirmed by using Fourier transform infrared (FT-IR) spectra and Raman spectrum. The FT-IR spectra of GO are presented in Figure 7a. The absorption bands at 1734, 1374, 1227, and 1061 $cm^{-1}$

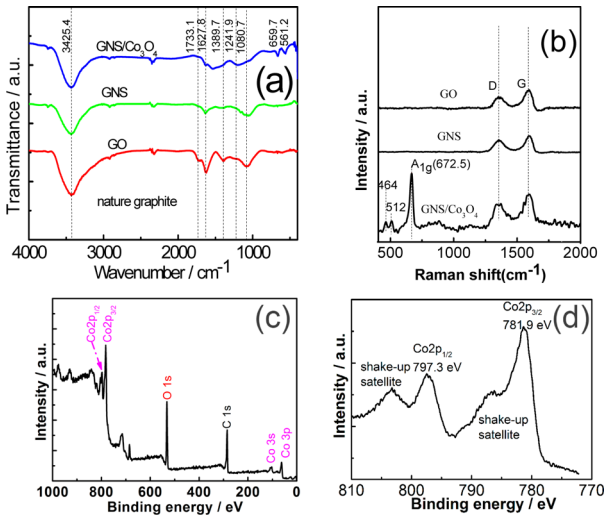


**Figure 7.** (a) FT-IR spectra of nature graphite, GO, GNS, and $Co_3O_4$/GNS; (b)Raman spectra of GNS, GO, and needle-like $Co_3O_4$/GNS composites; (c) XPS of the survey scan; and (d) Co 2p region of needle-like $Co_3O_4$/GNS composites.

can be assigned to the stretching vibrations of C═O, O—H, C—OH, and C—O, respectively. The absorption bands at 1624 $cm^{-1}$ can be attributed to the skeletal vibration of C═C from unoxidized graphitic domains, suggesting that the rich functional groups exist in the GO. However, only C═C, O—H, and C—OH bands can be seen in the FT-IR spectrum of GNS (Figure 7a) and the bands of C═O and C—O cannot be obviously observed, suggesting that GO is well reduced in the process of heat treatment.[34] For the FT-IR spectra of needle-like $Co_3O_4$/GNS, all the peaks of oxygen-containing functional groups corresponds to GNS, indicating that the GO in the composite has been reduced to GNS. Meanwhile, it can be clearly observed that there are two strong absorption bands at 659.7 and 561.2 $cm^{-1}$, which suggests the production of $Co_3O_4$.[35] In the Raman spectra of GO, GNS, and $Co_3O_4$/ GNS as shown in Figure 7b, the G band at around 1590 $cm^{-1}$ represents the $E_{2g}$ phonons of the C $sp^2$ atom,[36] while the D band at around 1330 $cm^{-1}$ is ascribed to defects like edges and disordered carbon.[37,38] In general, the intensity ratio of the D band and the G band ($I_D/I_G$) refers to the disorder density of carbon materials.[30] For the GO, the $I_D/I_G$ value is 0.9. Compared with that of GO, the $I_D/I_G$ of GNS decreased to 0.74 due to the reduced defects after the removal of oxygen-containing functional groups.[39] The $I_D/I_G$ value of needle-like $Co_3O_4$/GNS composites (0.72) is close to that of GNS (0.74), which suggests that GO in the needle-like composites reverted to GNS. The results are in good agreement with the results of FT-IR and XRD. The peaks located at 464 $cm^{-1}$, 512 $cm^{-1}$, and 672.5 $cm^{-1}$ can be assigned to the $E_{2g}$, $F_{2g}$, and $A_{1g}$ active modes of $Co_3O_4$,[36] respectively.

The chemical state of the elements in the composites is further characterized by X-ray photoelectron spectroscopy (XPS). The peaks located at 284.6 eV in Figure 7c can be assigned to the binding energy of C 1s of GNS. Co 2p XPS spectra as shown in Figure 7d have two main peaks with binding energy at 781.9 eV (Co $2p_{3/2}$) and 797.3 eV (Co $2p_{1/2}$). Two shakeup satellite peaks are located at about 6 eV above the main peaks. These results demonstrate that cobalt exists in the form of $Co_3O_4$. The detailed microscopic and spectroscopic results confirmed that the needle-like $Co_3O_4$ successfully deposited onto GNS.[35]

To test the electrochemical performance of needle-like $Co_3O_4$/GNS composites ($r_G/r_{Co}$ = 1:5), cyclic voltammogram (CV) is carried out in a three-electrode system using a SCE as the reference electrode and platinum foil as the counter-electrode. Figure 8a shows the CV of the needle-like $Co_3O_4$/

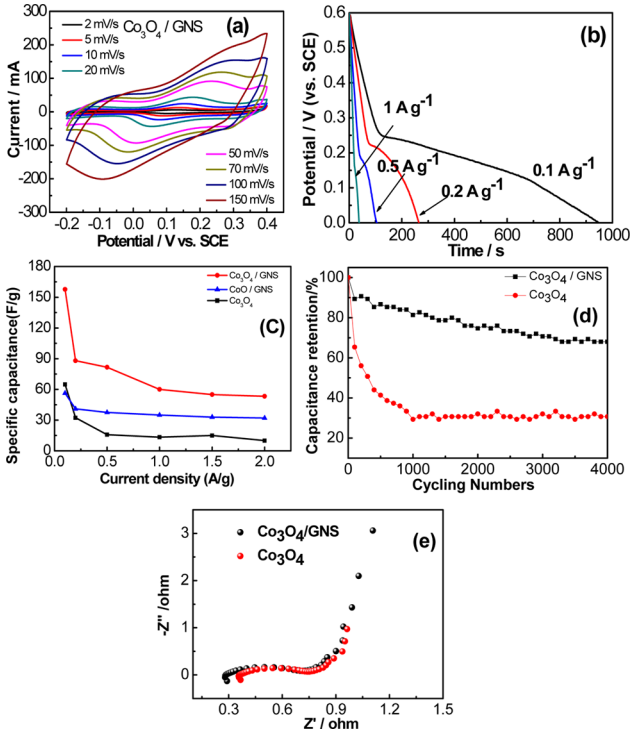


**Figure 8.** (a) Cyclic voltammograms of the needle-like $Co_3O_4$/GNS composites ($r_G/r_{Co}$ = 1:5) at different scan rates in 2 mol $L^{-1}$ KOH; (b) galvanostatic discharge curves of the $Co_3O_4$/GNS composite electrodes ($r_G/r_{Co}$ = 1:5) in 2 mol $L^{-1}$ KOH solution at 0.1 A $g^{-1}$ at different current densities; (c) galvanostatic specific capacitance retention of needle-like $Co_3O_4$/GNS ($r_G/r_{Co}$ = 1:5), CoO/GNS, and pure $Co_3O_4$ at different current densities; (d) average specific capacitance versus the cycle number of the pure $Co_3O_4$ and the needle-like $Co_3O_4$/GNS composites at a current density of 0.2 A $g^{-1}$; (e) Nyquist plots of pure $Co_3O_4$ and needle-like $Co_3O_4$/GNS composites.

GNS composites at different scan rates in a potential range of −0.2−0.4 V in 2 mol $L^{-1}$ KOH. It can be seen from the curves that the anodic peaks shifted toward positive potential and the cathodic peaks shifted toward negative potential with the increase of scan rate. The well-defined redox peaks in the CV curve are mainly attributed to the faradaic redox.[40] At low scan rate, the faradaic redox reaction is dependent on the insertion−deinsertion of protons in the electrolyte.

In order to determine the capacity of the composites, the galvanostatic charge−discharge curves of the $Co_3O_4$/ GNS composites ($r_G/r_{Co}$ = 1:5) and pure $Co_3O_4$ at a current density


dx.doi.org/10.1021/am5009369 | ACS Appl. Mater. Interfaces 2014, 6, 7626−7632

of 0.1 A $g^{-1}$ are shown in Supporting Information Figure S2. The discharge curves consist of a sudden potential drop around 0.35 V and a slow potential decay from 0.35 to 0.15 V. The composite electrode delivers a discharge capacitance of 157.7 F $g^{-1}$. The capacitance of the composites is remarkably enhanced compared with that of pure $Co_3O_4$ (77.2 F $g^{-1}$). It is in good agreement with the results of the CV curves. According to eq 1, the specific capacitances of $Co_3O_4$/GNS composites are calculated to be 157.7, 130.7, 88, 81.7, and 60 F $g^{-1}$ at a current density of 0.1, 0.2, 0.5, and 1 A $g^{-1}$, respectively (Figure 8b). As shown in Figure 8c, needle-like $Co_3O_4$/GNS shows better galvanostatic capacitance retention at different current densities from 0.1 A $g^{-1}$ to 2 A $g^{-1}$ compared with the CoO/GNS and pure $Co_3O_4$.

The long-term electrochemical capability of the electrode material is evaluated by conducting galvanostatic charge−discharge measurements at a current density of 0.2 A $g^{-1}$ in a potential range between 0 and 0.6 V. It can be seen from Figure 8d that the specific capacitance of needle-like $Co_3O_4$/GNS composites ($r_G/r_{Co}$ = 1:5) can maintain 70% of the initial value after 4000 cycles at 0.2 A $g^{-1}$, while pure $Co_3O_4$ only retained 30% after 4000 cycles at 0.2 A $g^{-1}$. The result demonstrates that the needle-like $Co_3O_4$/GNS composite has excellent cycle stability in the long term charge−discharge cycle test.

Electrochemical impedance spectroscopy (EIS) is carried out to further understand the fundamental behavior of supercapacitor electrodes. Figure 8e reveals the Nyquist plots of pure $Co_3O_4$ and needle-like $Co_3O_4$/GNS composite electrodes ($r_G/r_{Co}$ = 1:5). The plot is composed of a semicircle in the high frequency region and a straight line inclining about 45° to the real axis in the low-frequency region. The semicircle corresponds to double layer capacitance $C_{dl}$ and charge-transfer resistance $R_{ct}$. The straight line shows the Warburg impedance, which represents the electrolyte diffusion and proton diffusion in active materials.[38] From the plots, it can be seen that needle-like $Co_3O_4$/GNS composite has a smaller solution resistance, $R_s$ (0.28 Ω), and charge-transfer resistance, $R_{ct}$ (0.46 Ω), than pure $Co_3O_4$, suggesting that the needle-like $Co_3O_4$/GNS composite has better electrical conducting network due to the synergistic effect of graphene and cobalt oxide.

## 4. CONCLUSIONS

In summary, we demonstrate the preparation of the composites of needle-like $Co_3O_4$ anchored on the GNS with different mass ratios by a facile hydrothermal method. Graphene oxide nanosheets worked as the anchoring templates for in situ deposition of needle-like $Co_3O_4$. Without the template of graphene, the cobalt precursor tends to assemble into urchin-like spheres formed by many fine needles. When tested as the electrode material of aqueous supercapacitor, the composites of needle-like $Co_3O_4$/GNS ($r_G/r_{Co}$ = 1:5) exhibit obviously enhanced electrochemical performance with high capacitance retention of 70% over 4000 cycles. The synergistic effect of graphene and cobalt oxide in the unique multiscale structure of the composite may lead to the enhancement of excellent electrochemical performances.

## ■ ASSOCIATED CONTENT

### Supporting Information

Galvanostatic discharge curves of the pure $Co_3O_4$ and $Co_3O_4$/GNS composite electrodes and the $N_2$ adsorption−desorption isotherm of the composites sample obtained after annealing at different temperatures. This material is available free of charge via the Internet at http://pubs.acs.org.

## ■ AUTHOR INFORMATION

### Corresponding Authors

*E-mail: edward.bwang@gmail.com (B. Wang). Fax: +86 816-2544426.

*E-mail: niefude@caep.ac.cn (F.D. Nie). Fax: +86 816-2544426.

### Notes

The authors declare no competing financial interest.

## ■ ACKNOWLEDGMENTS

This work was supported by the Startup Foundation of China Academy of Engineering Physics, Institute of Chemical Materials (KJCX201301 and KJCX201306) and National High-tech Research and Development Program (863 Program: No. 2013AA050905).

## ■ REFERENCES

(1) Sun, Y.; Wu, Q.; Shi, G. Graphene Based New Energy Materials. *Energy Environ. Sci.* **2011**, *4*, 1113−1132.

(2) Xie, L. J.; Wu, J. F.; Chen, C. M.; Zhang, C. M.; Wan, L.; Wang, J. L.; Kong, Q. Q.; Lv, C. X.; Li, K. X.; Sun, G. H. A Novel Asymmetric Supercapacitor with an Activated Carbon Cathode and a Reduced Graphene Oxide-Cobalt Oxide Nanocomposite Anode. *J. Power Sources* **2013**, *242*, 148−156.

(3) Du, W.; Liu, R.; Jiang, Y.; Lu, Q.; Fan, Y.; Gao, F. Facil Synthesis of Hollow $Co_3O_4$ Boxes for High Capacity Supercapacitor. *J. Power Sources* **2013**, *227*, 101−105.

(4) Wang, G.; Zhang, L.; Zhang, J. A Review of Electrode Materials for Electrochemical Supercapacitors. *Chem. Soc. Rev.* **2012**, *41*, 797−828.

(5) Du, X.; Wang, C.; Chen, M.; Jiao, Y.; Wang, J. Electrochemical Performances of Nanoparticle $Fe_3O_4$ /Activated Carbon Supercapacitor Using KOH Electrolyte Solution. *J. Phys. Chem. C* **2009**, *113*, 2643−2646.

(6) Kaempgen, M.; Chan, C. K.; Ma, J.; Cui, Y.; Gruner, G. Printable Thin Film Supercapacitors Using Single-walled Carbon Nanotubes. *Nano Lett.* **2009**, *9*, 1872−1876.

(7) Hu, C. C.; Chang, K. H.; Lin, M. C.; Wu, Y. T. Design and Tailoring of the Nanotubular Arrayed Architecture of Hydrous $RuO_2$ for Next Generation Supercapacitors. *Nano Lett.* **2006**, *6*, 2690−2695.

(8) Feng, X. Y.; Shen, C.; Yu, Y.; Wei, S. Q.; Chen, C. H. Synthesis and Electrochemical Properties of Sticktight-Like and Nanosheet $Co_3O_4$ Particles. *J. Power Sources* **2013**, *230*, 59−65.

(9) Chen, S.; Zhu, J.; Wu, X.; Han, Q.; Wang, X. Graphene-$MnO_2$ Nanocomposites for Supercapacitors. *ACS Nano* **2010**, *4*, 2822−2830.

(10) Vijayakumar, S.; Nagamuthu, S.; Muralidharan, G. Supercapacitor Studies on NiO Nanoflakes Synthesized Through a Microwave Route. *ACS Appl. Mater. Interfaces* **2013**, *5*, 2188−2196.

(11) Li, X.; Shao, J.; Li, J.; Zhang, L.; Qu, Q.; Zheng, H. Ordered Mesoporous $MoO_2$ as a High-Performance Anode Material for Aqueous Supercapacitors. *J. Power Sources* **2013**, *237*, 80−83.

(12) Liu, X.; Long, Q.; Jiang, C.; Zhan, B.; Li, C.; Liu, S.; Zhao, Q.; Huang, W.; Dong, X. Facile and Green Synthesis of Mesoporous $Co_3O_4$ Nanocubes and Their Application for Supercapcitors. *Nanoscale* **2013**, *5*, 6525−6529.

(13) Xia, X. H.; Tu, J. P.; Wang, X. L.; Gu, C. D.; Zhao, X. B. Mesoporous $Co_3O_4$ Monolayer Hollow-Sphere Array as Electrochemical Pseudocapacitor Material. *Chem. Commun.* **2011**, *47*, 5786−5788.

(14) Xiao, Y.; Liu, S.; Li, F.; Zhang, A.; Zhao, J.; Fang, S.; Jia, D. 3D Hierachical $Co_3O_4$ Twin-Spheres with an Urchin-Like Structure: Large-Scale Synthesis, Multistep-Splitting Growth, and Elctrochemical Pseudocapacitors. *Adv. Funct. Mater.* **2012**, *22*, 4052−4059.

(15) Zhou, W.; Liu, J.; Chen, T.; Tan, K. S.; Jia, X.; Luo, Z.; Cong, C.; Yang, H.; Li, C. M.; Yu, T. Fabrication of $Co_3O_4$-Reduced Graphene Oxide Scrolls for High-Performance Supercapacitor Electrodes. *Phys. Chem. Chem. Phys.* **2011**, *13*, 14462−14465.
(16) Liu, G. J.; Fan, L. Q.; Yu, F. D.; Wu, J. H.; Liu, L.; Qiu, Z. Y.; Liu, Q. Facile One-Step Hydrothermal Synthesis of Reduced Graphene Oxide/$Co_3O_4$ Composites for Supercapacitors. *J. Mater. Sci.* **2013**, *48*, 8463−8470.
(17) Guo, S.; Dong, S. Graphene Nanosheet: Synthesis, Molecular Engineering, Thin Film, Hybrides, and Energy and Analytical Applications. *Chem. Soc. Rev.* **2011**, *40*, 2644−2672.
(18) Geim, A. K.; Novoselov, K. S. The Rise of Graphene. *Nat. Mater.* **2007**, *6*, 183−191.
(19) Huang, X.; Qi, X.; Boey, F.; Zhang, H. Graphene-Based Composites. *Chem. Soc. Rev.* **2012**, *41*, 666−686.
(20) Cao, X.; Shi, Y.; Shi, W.; Lu, G.; Huang, X.; Yan, Q.; Zhang, Q.; Zhang, H. Preparation of Novel 3D Graphene Networks for Supercapacitor Applications. *Small* **2011**, *7*, 3163−3168.
(21) Chen, Y.; Zhang, X.; Yu, P.; Ma, Y. Electrophoretic Deposition of Graphene Nanosheets on Nickel Foams for Electrochemical Capacitors. *J. Power Sources* **2010**, *195*, 3031−3035.
(22) Vivekchand, S. R. C.; Rout, C. S.; Subrahmanyam, K. S.; Govindaraj, A.; Rao, C. N. R. Graphene-based Electrochemical Supercapacitors. *J. Chem. Sci.* **2008**, *120*, 9−13.
(23) Zhou, W.; Liu, J.; Chen, T.; Tan, K. S.; Jia, X.; Luo, Z.; Cong, C.; Yang, H.; Li, C. M.; Yu, T. Fabrication of $Co_3O_4$-reduced Graphene Oxide Scrolls for High- performance Supercapacitor Electrodes. *Phys. Chem. Chem. Phys.* **2011**, *13*, 14462−14465.
(24) Cheng, J. L.; Xin, H. L.; Zhang, H. M.; Wang, B. One-pot Synthesis of Carbon Coated-$SnO_2$ /Graphene-Sheet Nanocomposite with Highly Reversible Lithium Storage Capability. *J. Power Sources* **2013**, *232*, 152−158.
(25) Cheng, J. L.; Wang, B.; Xin, H. L.; Yang, G. C.; Cai, H. Q.; Nie, F. D.; Huang, H. Self-assembled $V_2O_5$ Nanosheets/Reduced Graphene Oxide Hierarchical Nanocomposite as a High-performance Cathode Material for Lithium Ion Batteries. *J. Mater. Chem. A* **2013**, *1*, 10814−10820.
(26) Li, D.; Muller, M. B.; Gilje, S.; Kaner, R. B.; Wallace, G. G. Processable Aqueous Dispersions of Graphene Nanosheets. *Nat. Nanotechnol.* **2008**, *3*, 101−105.
(27) Wang, M.; Huang, J.; Wang, M.; Zhang, D.; Zhang, W.; Li, W.; Chen, J. $Co_3O_4$ Nanorods Decorated Reduced Graphene Oxide Composite for Oxygen Reduction Reaction in Alkaline Electrolyte. *Electrochem. Commun.* **2013**, *34*, 299−303.
(28) Liang, Y. Y.; Wang, H. L.; Zhou, J. G.; Wan, J.; Regier, T. $Co_3O_4$ Nanocrystals on Graphene as a Synergistic Catalyst for Oxygen Reduction Reaction. *Nat. Mater.* **2011**, *10*, 780−786.
(29) Zhou, G.; Wang, D. W.; Li, F.; Zhang, L.; Li, N.; Wu, Z. S.; Wen, L.; Lu, G. Q.; Cheng, H. M. Graphene-Wrapped $Fe_3O_4$ Anode Material with Improved Reversible Capacity and Cyclic Stability for Lithium ion Batteries. *Chem. Mater.* **2010**, *22*, 5306−5313.
(30) Wang, X.; Liu, S.; Wang, H.; Tu, F.; Fang, D.; Li, Y. Facile and Green Synthesis of $Co_3O_4$ Nanoplates/Graphene Nanosheets Composite for Supercapacitor. *J. Solid State Electrochem.* **2012**, *16*, 3593−3602.
(31) Xu, C.; Wang, X.; Zhu, J.; Yang, X.; Lu, L. Deposition of $Co_3O_4$ Nanoparticles onto Exfoliated Graphite Oxide Sheets. *J. Mater. Chem.* **2008**, *18*, 5625−5629.
(32) Wang, J.; Zheng, S.; Shao, Y.; Liu, J.; Xu, Z.; Zhu, D. Amino-functionalized $Fe_3O_4$@$SiO_2$ Core-shell Magnetic Nanomaterial as a Novel Adsorbent for Aqueous Heavy Metals Removal. *J. Colloid Interface Sci.* **2010**, *349*, 293−299.
(33) Rui, X. H.; Tan, H. T.; Si, D. H.; Liu, W. L.; Xu, C.; Hng, H. H.; Yazami, R.; Yan, Q. Y. Tempalte-free Synthesis of Urchin-like $Co_3O_4$ Hollow Spheres with Good Lithium Storage Properties. *J. Power Sources* **2013**, *222*, 97−102.
(34) Yue, W. B.; Jiang, S. H.; Yang, X. J. Preparation of Graphene-encasulated Mesoporous Metal Oxides and Their Application as Anode Materials for Lithium-ion Batteries. *J. Mater. Chem.* **2012**, *22*, 16318−16323.
(35) Huang, S.; Jin, Y.; Jia, M. Preparation of Graphene/ $Co_3O_4$ Composites by Hydrothermal Method and Their Electrochemical Properties. *Electrochim. Acta* **2013**, *95*, 139−145.
(36) Cheng, J. L.; Wang, B.; Park, C. M.; Wu, Y. P.; Huang, H.; Nie, F. D. CNT@$Fe_3O_4$@C Coaxial Nanocables: One-Pot, Additive-Free Synthesis and Remarkable Lithium Storage Behavior. *Chem.—Eur. J.* **2013**, *19*, 9866−9874.
(37) Chen, Y.; Tang, X. S.; Li, L. B.; Xue, J. M. One-step Synthesis of Hollow Porous $Fe_3O_4$ Beads-reduced Graphene Oxide Composites with Superior Battery Performance. *J. Mater. Chem.* **2012**, *22*, 17656−17662.
(38) Cheng, J. L.; Wang, B.; Xin, H. L.; Kim, C.; Nie, F. D.; Yang, G. C.; Huang, H. Conformal Coating of $TiO_2$ Nanorods on a 3-D CNT Scaffold by Using a CNT Film as a Nanoreactor: a Free-standing and Binder-free Li-ion Anode. *J. Mater. Chem. A* **2013**, *2*, 2701−2707.
(39) Gao, W.; Alemany, L. B.; Ci, L.; Ajayan, P. M. New Insights into the Structure and Reduction of Graphite Oxide. *Nat. Chem.* **2009**, *1*, 403−408.
(40) Zhang, G.; Wang, T.; Yu, X.; Zhang, H.; Duan, H.; Lu, B. Nanoforest of Hierarchical $Co_3O_4$ @$NiCo_2O_4$ Nanowire Arrays For High-performance Supercapacitors. *Nano Energy* **2013**, *2*, 586−594.